Simulation and Analysis of NASA Lift Plus Cruise eVTOL Crash Test

Jacob Putnam
Jacob.B.Putnam@nasa.gov
Research Aerospace Engineer
NASA Langley Research Center
Hampton VA, 23681

Justin Littell
Justin.D.Littell@nasa.gov
Research Aerospace Engineer
NASA Langley Research Center
Hampton VA, 23681

ABSTRACT

The National Aeronautics and Space Administration (NASA) conducted a full-scale crash test of a representative electric vertical take-off and landing (eVTOL) fuselage in November 2022. The test article was a carbon-composite fuselage cabin section of the six-passenger lift plus cruise (LPC) eVTOL design concept which was created by NASA researchers to advance understanding of eVTOL propulsion, noise, and safety. The fuselage cabin section was impacted onto a concrete surface with a combined horizontal and vertical velocity approximating a severe but survivable crash landing. This test was conducted to generate data to help inform eVTOL crashworthiness regulation development, evaluate the use of energy absorbing (EA) concepts within vehicle design, and quantify the predictive accuracy finite element (FE) modelling techniques used in crashworthiness predictions. The response of the eVTOL representative fuselage when subjected to dynamic impact loading was evaluated through structural instrumentation, anthropometric test devices (ATDs), and high-speed photogrammetry. The development of a representative FE model of the test article and comparison between model to test results is described within this manuscript to quantify the capability of these tools to predict crashworthiness of the carbon-composite eVTOL airframe.

A FE model of the LPC test article was generated to match the structural geometry, fabrication specifications, materials, and component layout of the test article. Representative material models were generated for the composite materials used within the test article using coupon and component material characterization test data. The developed model was simulated in the recorded test impact conditions. The developed model predicted the initial accelerative load transferred from the ground impact into the vehicle structure but did not predict brittle failure of the composite structure to the extent which was observed in test. Post-test calibration of the model showed that tuning of the failure parameters within the composite structure material model was needed to more accurately predict the structural damage observed in test. In addition, it was found that inclusion of full ATD models within the vehicle simulation, rather than using representative point masses, resulted in improved prediction of vehicle structural response. The post-test calibrated model was shown to closely predict occupant injury risk measured during the test giving confidence in the use of the developed model to predict these metrics for EA component development going forward.

INTRODUCTION

The electric Vertical Take-off and Landing (eVTOL) industry aims to bring aerial transportation to the urban environment using novel electrified vehicle designs. eVTOL vehicles are characterized by their lightweight structures, use of non-traditional materials, and unique flight profiles. eVTOL manufacturers are in various stages of development and production, with released designs showing a range of features including multiple engine and rotor combinations, fixed and vertical lift structures, and varied cabin configurations. These designs do not adhere to standard design paradigms of traditional General Aviation (GA) or rotorcraft vehicles. Thus, a concerted effort is needed to characterize the behavior of these vehicle architectures in order to insure they meet the degree of safety and reliability required to achieve public acceptance.

The current standards for GA and rotorcraft are based on mishap data, full-scale testing, and other historical factors from 50+ years of service. The available data for eVTOL designs is limited in comparison. To progress the eVTOL design knowledge base, the National Aeronautics and Space Administration (NASA) has conducted a full-scale dynamic impact test of an eVTOL design concept. This test was conducted to advance the eVTOL industry by

providing relevant data on eVTOL crashworthiness to manufacturers, regulators, academia, and other interested parties within the general public.

The NASA eVTOL dynamic impact test was performed using a test article designed from the NASA Lift plus Cruise (LPC) vehicle architecture [1]. This vehicle architecture has been used as the basis for dynamic environments research conducted at NASA because it shares design features that are commonly associated with numerous eVTOL vehicles currently in design. These common features include a high wing design with multiple lifting sources, a large cabin capable of seating six occupants, and a lightweight composite material structure. Additionally, the design is open source and design characteristics are able to be shared with the eVTOL community. The NASA LPC vehicle concept is shown in Figure 1.

Figure 1. NASA Lift Plus Cruise (LPC) concept vehicle.

Alongside the physical test, a finite element (FE) model of the LPC test article configuration was generated using the commercially available FE analysis code LS-DYNA. This model was used to guide the test article development as well as assess the capability of FE analysis to predict crashworthiness in an eVTOL relevant design. FE analysis has enormous potential to improve vehicle capability through design optimization and potentially reduce vehicle certification cost by supplementing the test requirement burden. To achieve this potential, the capabilities, limitations, best practices of current modeling tools need to be thoroughly characterized and agreed upon. The current study aims to provide data and insights into FE model prediction of eVTOL crashworthiness to improve understanding of these tools.

MODEL DEVELOPMENT

LPC Structural Model

The LPC test article was generated from the LPC vehicle concept by simplifying the flight components and maturing the structural design of the vehicle cabin. Flight components were reduced to mass representations, with the largest changes being the reduction of the wing and tail

sections of the vehicle. Comparison of the flight design and test article design, demonstrating this simplification, is provided in Figure 2. A detailed description of the conversion of the LPC vehicle to test article design can be found in [2].
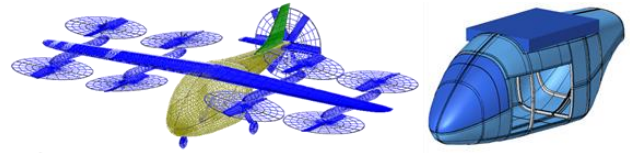

Figure 2. LPC flight design (left) and test article design (right).

A FE model of the LPC test article was generated to define the structural design and fabrication requirements of the test article. Test article composite structure were sized to meet Federal Aviation Administration (FAA) rotorcraft inertial load requirements described in Code of Federal Regulations (CFR) 27.561 [3]. Details on the development of- and analysis performed with- this structural sizing model can be found in [2]. The structural sizing analysis was conducted prior to test article fabrication and thus the sizing model did not contain nuanced material, fabrication, and assembly details that went into the fully fabricated test article. The following minimum structural design requirements were generated from this analysis: six- and eight-layer 3K PW carbon composite in a [0°/45°] layup for the skin and frames respectively, a 10-ksi strength resin, and a 2.9-ksi bond strength on post-cure bonds.

Based on the design requirements developed, the test article skin and frame sections were fabricated from 3K-70-PW carbon fabric infused with INF-114 resin and cured at room temperature under vacuum. This specific material system is referred to as C/C throughout this manuscript. Flat sheet samples of both the skin and frame layups were fabricated using the same methodology used in the vehicle fabrication for material model characterization testing. Static tension and compression tests were performed on ASTM D3039 [4] coupon specimens cut from the sample sheets. A model of the C/C material system was generated from these coupon tests. All composite material models described within this manuscript were generated using *MAT_58: Laminated Composite Fabric and all composite layup definitions were implements using *PART_COMPOSITE within LS-DYNA.Results of the tensile coupon tests and correlation of the calibrated material model to test are shown in

Figure **3**. A total of 17 tests were performed in summation of the six- and eight- layer coupons. Tests showed consistent material response under tensile load. The calibrated material model closely predicted the material response measured under static tensile loading
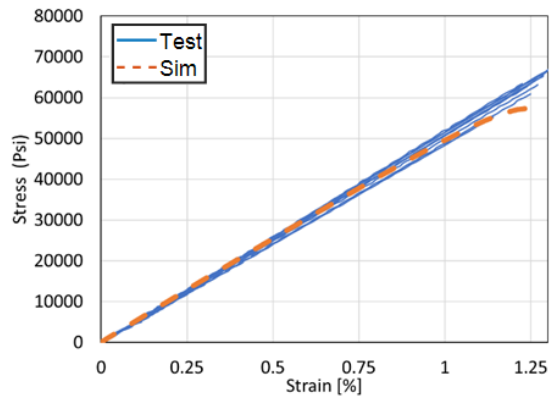
Figure 3. Tensile coupon test results and model correlation for C/C material.

Results of the static compression coupon tests performed, and the correlation of the calibrated material model are shown in Figure 4. The compression test data was more inconsistent than the tensile data. Several tests were removed due to incongruent results leaving a total of four response curves with which to calibrate the material model under compressive loading of the composite material under compression. From these tests, non-linear stress limits and compressive strength/strain parameters were estimated.
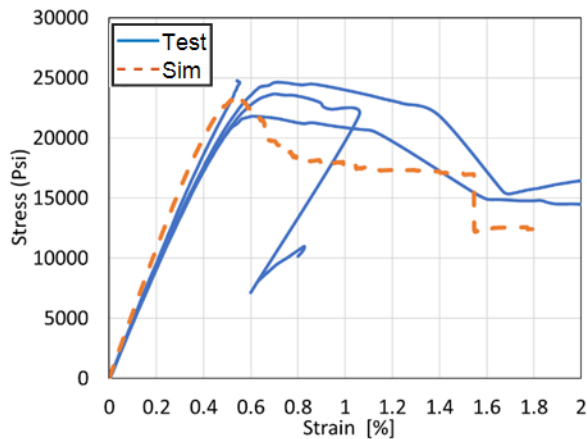

Figure 4. Compression coupon test results and model correlation for C/C material.

The skin and frames of the LPC test article structure were co-cured in four large sections during fabrication. This methodology was used, rather than fabricating the frames and skin separately, with the intent of minimizing the amount of post-cure bonded parts within the structure. Each section was fabricated such that there was an overlapping skin portion which would be used to bond the sections together. Sections were bonded together using LORD® 320/322 adhesive. A schematic of the LPC assembly design is shown in Figure 5. In addition to the composite structure, a 1/8-in. acrylic windscreen was formed at the front of the cabin and fixed to the structure using a combination of 3M™ Aerospace Sealant AC-251 and fasteners.
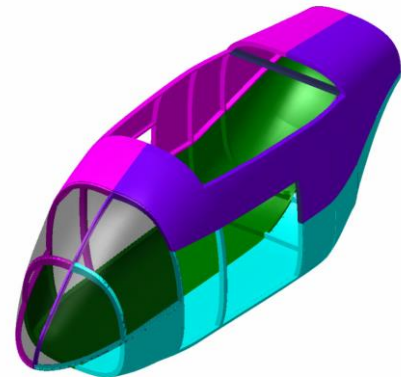

Figure 5. LPC test article assembly design.

An FE model of the as-built LPC test article was generated utilizing the finalized material, fabrication, and assembly details. To represent the sectioned fabrication approach, the preliminary FE model of the LPC test article, used in sizing analysis, was adjusted. The FE model was split into the four fabricated sections, each with a newly assigned part number. The overlapped skin sections were then added to the model and the sections were attached using *CONTACT TIED SURFACE TO SURFACE FAILURE within LS-DYNA. Contact failure was defined at 4500 psi, per the manufacturer specifications of the LORD® 320/322 adhesive used in assembly. An elastic-plastic material model, *MAT_3: Plastic Kinematic, of the acrylic windscreen was generated from manufacturer specifications. The windscreen model was fixed to the structure through a combination of tied surface contact with failure and constrained nodal rigid bodies (CNRBs) representing the sealant and fasteners used in assembly. To accommodate greater detail in the as built LPC test article model the mesh density was refined to 0.5 in., as compared to the 1.0 in. mesh used in the preliminary sizing analysis. The FE model of the as-fabricated LPC test article design is shown in Figure 6, noting each part within the model is a different color.
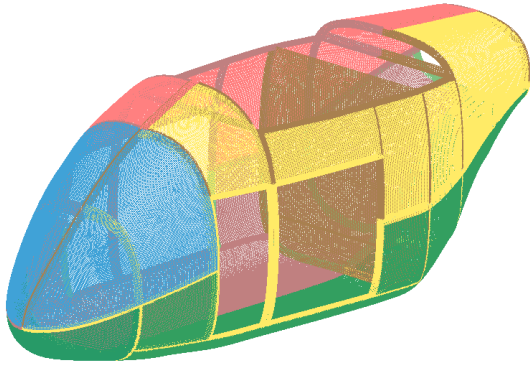
Figure 6. LPC test article structural model.

LPC Component Models

The floor of the LPC test article was made using lightweight carbon composite construction. The floor was composed of a sandwich composite with four layers of carbon fiber face sheets around a closed cell rigid polyurethane foam core. A static three-point bend test was performed on the floor sections to characterize the sandwich composite stiffness The test and simulation of the three-point bend test is shown in Figure 7.
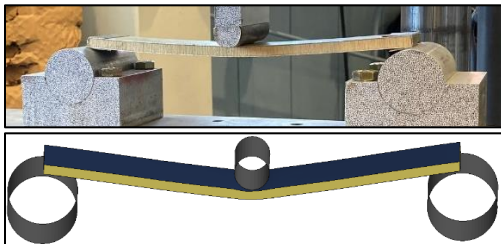

Figure 7. LPC floor three-point bend test setup (top) and simulation (bottom).

Data from the static three-point bend testing performed on the floor section was used to calibrate a representative FE model of the floor. The sandwich composite floor was modeled utilizing shell elements for the composite skin and solid elements for the polyurethane foam core. The polyurethane material was modeled as *MAT_63: Crushable Foam. A mesh length of 1.0 in. was used throughout the floor model.

Correlation between the developed model and floor specimen within the three-point bend test configuration is shown in Figure 8. The force displacement response of the floor was closely predicted by the representative model. The response slope was precisely replicated, indicating representation of the sandwich composite stiffness. Failure of the test specimen occurred at a displacement approximately 0.01 in. less than the model prediction indicating a slight overestimation of floor strength by the model. Calibration was attempted to improve this discrepancy, but no realistic solution was identified which would improve the failure prediction without reducing correlation of the stiffness prediction. Point failure of the floor was not expected during the vehicle test conditions and thus this slight discrepancy in failure strength was considered acceptable.
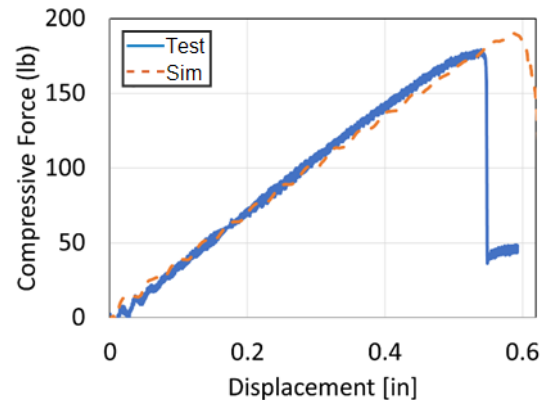

Figure 8. LPC floor three-point bend test results and model correlation.

Energy absorbing (EA) component mechanisms were integrated into the subfloor and seat systems within the LPC test article in order to assess their capability in an eVTOL relevant dynamic impact environment. The EA mechanisms were fabricated out of hybrid carbon-Kevlar® composite material, composed of plain weave of 3k sized carbon fibers in the warp direction and 3k sized aramid fibers in the fill direction. This material system will be referred to as C/K throughout the manuscript. The combination of carbon and Kevlar® weaves result in a strong, lightweight, and ductile material. The strength and ductility provide energy absorption capability through high-strength material bending and crushing, without the brittle failure associated with an all-carbon composite. The lightweight aspect of the material makes it ideal for EA components within aerospace structures. NASA has previously studied this material for use both traditional rotorcraft and eVTOL EA component designs [5-9].

The C/K material system used in the EA component mechanisms studied within the LPC test article has been characterized through of building block testing carried out at NASA Langley Research Center (LaRC) [5,6]. The majority of those studies were performed using West Systems 105/205 resin. For the purposes of the LPC test, a higher strength resin system, Epon 828 (E828), was used in the fabrication of the EA components.

A material model of the C/K material system with E828 resin was developed through static material coupon testing. Detailed description of the testing and developed model

correlation can found in [9]. Example correlation to tensile stress-strain response of coupon specimens cut at 45° is shown in Figure 9. The developed material model predicted both linear elastic and non-linear stress-strain response of the tested specimens. These results provided confidence that the developed material was accurately capturing the stiffness and strength characteristics of the composite material system.
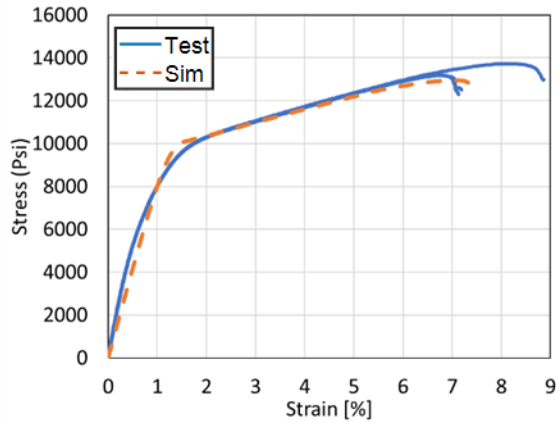

Figure 9. Tensile 45° coupon test results and model correlation for C/K material.

Component level testing was performed using the EA mechanisms fabricated with the C/K material system in order to verify the composite damage and failure response predictions made using the developed material model. The EA subfloors generated for the LPC test article were designed as modular standalone components independent from the vehicle structure. This design path was selected over a traditional rotorcraft bulkhead keel beam structure as it allows for greater weight and space optimization capability and integration into non-traditional fuselage shapes within the eVTOL design space. The EA subfloors designed for this application were made in a laterally braced cruciform geometry with corrugated walls. The subfloor design is shown in Figure 10. The cruciform shape of the subfloor design provides standalone rigidity to the component which allows it to be modularly placed within the subfloor space without reliance on the fuselage structure and to withstand shear loading induced from horizontal impact conditions. The corrugated walls reduce crush initiation force and stabilize the crush response of the cruciform walls improving EA efficiency.
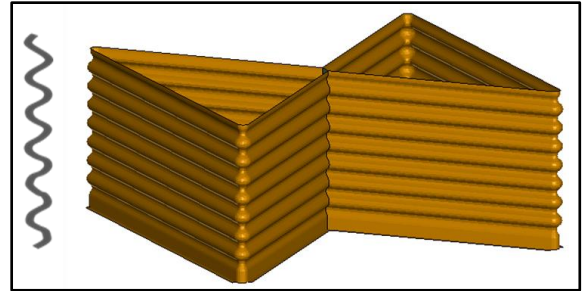

Figure 10. EA subfloor design.

A preliminary design study was carried out to characterize the capability of the cruciform subfloor design when subjected to single and multi-axis loading environments. This study also characterized effects of wall geometry and composite layup on EA response. A detailed overview of this study and outcomes can be found in [9]. Results of this characterization study were used to select the subfloor wall geometry and composite layups used in the LPC test article.

The EA cruciform subfloors were fabricated using the C/K material system oriented at 45°, vacuum bagged and cured at room temperature with E828 resin. A total of nine cruciform subfloors were fabricated and integrated into the LPC test article. Six subfloors composed of four composite layers were fabricated and integrated under each seat within the LPC test article. For additional support, two five-layer subfloors were fabricated to go under the data acquisition system (DAS) and a single five-layer was integrated under the floor section forward of the front row of seats.

Component level test drop tower tests were conducted with both the four-layer and five-layer subfloor configurations fabricated for the LPC test article. For each test, a 175 lb. rigid steel mass, representative of a mid-size male occupant, was dropped onto the subfloor component with an impact speed of 22 ft/s. Acceleration time history of the impactor and high-speed photogrammetry were recorded during each test. This data was compared against FE simulations of the tested conditions in order to assess predictive accuracy of the C/K material system and representative subfloor component model. The subfloor component model was composed of shell elements with a mesh length of 0.1 in. and utilized the C/K with E828 material model previously generated. The drop test configuration and representative model is shown in Figure 11.
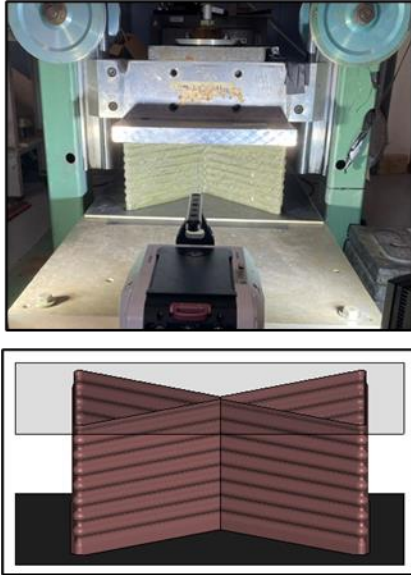
Figure 11.EA subfloor component test (top) and simulation (bottom) setup.

Comparison of the predicted and recorded impactor acceleration time history during the 4-layer subfloor drop tower test is shown in Figure 12. The FE model closely predicted the impactor acceleration time history during crushing of the subfloor but overpredicted acceleration during initial contact with the impactor. The overprediction of initial acceleration was not observed in the 5-layer test. Material model tuning was explored to reduce the overprediction of initial acceleration, but no effective material calibration solution was found. The parameter found most effective at improving this response was scaling the contact penalty stiffness between impactor and subfloor. Although this was identified as a potential method for improving correlation to this test, no scaling of the contact penalty stiffness was ultimately performed. The test data set was not robust enough to validate any tuning of this potentially non-physical parameter. In addition, tuning the model for this contact effect had minimal value for the integrated vehicle system analysis in which a tied contact was used between the vehicle, subfloor, and floor elements.
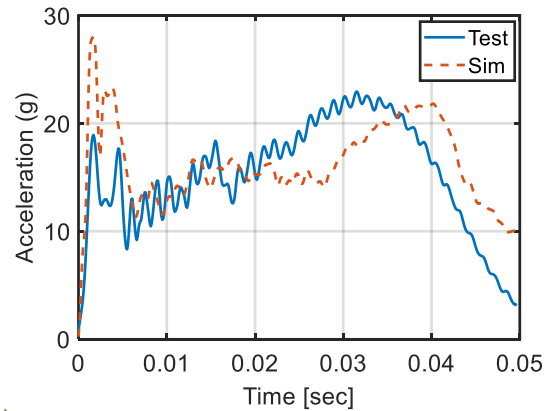

Figure 12. EA subfloor 4-layer component test results and model correlation.

Comparison of the predicted and recorded impactor acceleration time history during the five-layer subfloor drop tower test is shown in Figure 13. Unlike the four-layer configuration, the five-layer model closely predicted the initial impact acceleration but underpredicted acceleration during crush. Results of the four- and five-layer subfloor correlation indicate reasonable prediction of the overall crush response of the subfloor component with room for improvement with additional test data. Additional component tests are planned to identify potential variability in crush response of the fabricated design and further ground the developed FE models.
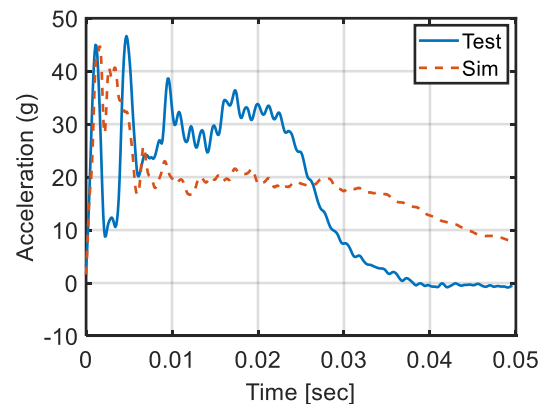

Figure 13. EA subfloor five-layer component test results and model correlation.

Four rigid and two EA seats were integrated into the LPC test article. Five of the seats used in the test were assembled by NASA utilizing generic commercial off the shelf (COTS) seat buckets and custom fabricated aluminum frames. The remaining seat was a complete COTS seat. A representative FE model of each seat design was generated using a combination of three-dimensional (3D) scans and hand measurements. The seat buckets were meshed using

shell elements with a mesh density of 1.0 in. For the rigid seat designs, the frames were represented through rigid nodal attachments between the floor seat track and the seat pan models. For the NASA EA seat, the EA components were explicitly represented through meshed elements while the support frame was represented through a combination of joint elements and rigid nodal attachments. The NASA EA seat and representative model is shown in Figure 14.
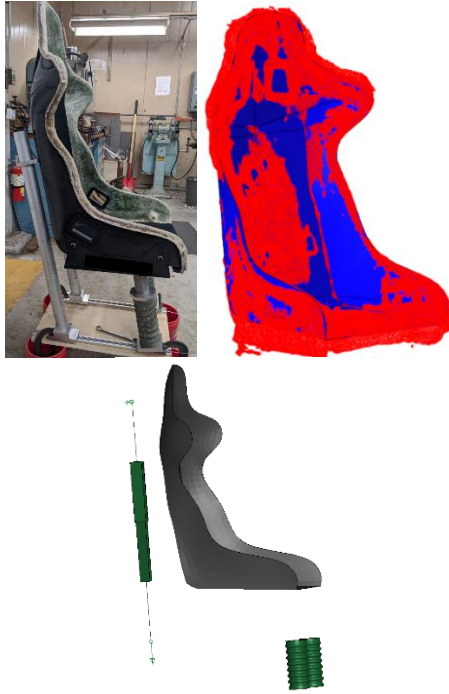

Figure 14. NASA EA seat design and representative model.

The NASA EA seat design utilized crush tubes, composed of the C/K material, integrated into the seat frame. The walls of the crush tubes were designed in an accordion shape which reduced crush initiation force on the tube and stabilized the folding mechanism of the tube during crush. Additional detail on the development and analysis of this EA tube design can be found in [6-8].

Two crush tubes were used in the NASA EA seat; each were integrated into the forward leg supports with a sliding plunger mechanism on the legs designed to crush into the tubes during vertical loading. The crush tubes were fabricated using four layers of C/K material system oriented in a repeating $[+45°/- 45°]_2$ layup, vacuum bagged and cured at room temperature with E828 resin. FE models were generated matching the geometry of the tubes, using shell elements with a mesh length of 0.1 in.

Prior to integration within the test article, component level drop tower testing was performed on the as-fabricated crush tube design. Tests were performed with a 100 lb. mass impacting the crush tube with a vertical velocity of 20 ft/s. The component test conditions were simulated with the representative FE tube model to assess the predictive accuracy of the model.

Acceleration time history of the drop mass during impact with the crush tube is compared between test and simulation in Figure 15. Impactor acceleration was closely predicted by the FE model during EA tube crushing, while initial impact acceleration was slightly over predicted. This correlation result closely resembles the correlation observed in the four-layer subfloor component test predictions. Similar to the subfloor, the initial overprediction of acceleration was correlated to the contact stiffness between the shell edge of the crush tube and rigid impactor. Barring this contact effect, which was not relevant to the integrated seat model setup, the crush tube model prediction provided confidence in its realistic prediction of the crush response of the physical component.
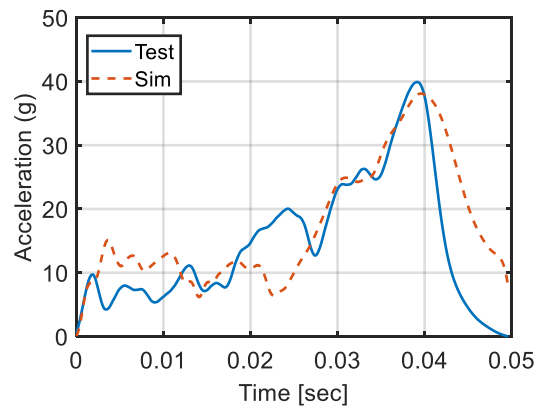

Figure 15. EA crush tube component test results and model correlation.

The floor, subfloor, and seat component models were integrated into the FE model of the LPC test article matching the setup used in testing. The final model configuration is shown in Figure 16. The nine subfloor components were fixed to the belly skin of the LPC and the floor using a combination of rivets and adhesive. This was represented within the model through tied contacts defined between these three component models. The subfloor models were aligned with one four-layer subfloor under each seat location as it was configured within the test. Aluminum beam elements were defined along the floor length representing the seat tracks used in test. These elements were fixed to the floor using CNRBs representative of nut-bolt attachments used in the test article. The individual seat models were fixed to rigid sections defined on the seat tracks at the seat frame attachment locations, using constrained nodal sets between parts.
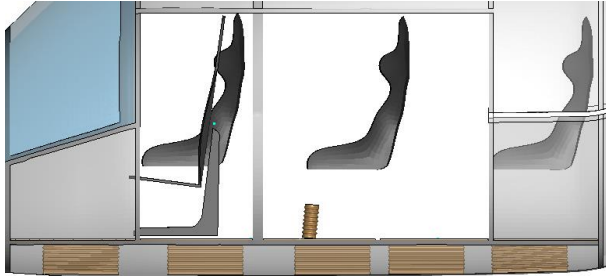
Figure 16. LPC test article cabin configuration.

Six Anthropomorphic Test Devices (ATDs) were integrated within the LPC test article. Two Hybrid III FAA 50th (H3 50th FAA), one Hybrid II 50th (H2 50th), one Hybrid III 95th (H3 95th), one Hybrid III 5th (H3 5th), and one Hybrid III 10-year-old (H3 10 YO) were tested. The configuration of these ATDs within the test article is shown in Figure 17, with the left side of the figure being the forward end of the test article. For the pre-test prediction analysis point masses were rigidly fixed to the seat models to represent the weight of each ATD within the seat. Pre-test analyses were focused on vehicle structural response and thus the ATD models were not included within the pre-test simulations in order to reduce computation time required for simulation.
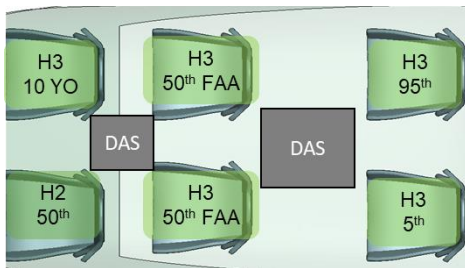

Figure 17. LPC test article ATD layout.

A three-in. x three-in. steel box beam welded frame was fabricated and mounted to the Wingbox area of the LPC test article. This welded steel structure served two purposes; it served as lifting hardware and as mass representative of the wings, flight hardware, and batteries. During the test article sizing analysis, the wings and flight hardware were represented using simplified beam structures with attached weight. In the as-tested configuration this design was further simplified to the steel frame shown in Figure 18. This was done to streamline the test setup and improve safety margin on the lifting hardware. An FE model of the lifting hardware was generated using beam elements matching the specifications of the fabricated hardware. The component was fixed to the LPC test article model using constrained nodal sets representative of the bolted connections between the lifting hardware and the test article frame. Using the updated lifting hardware model, pre-test simulations were conducted and showed the cabin volume

to be maintained with the changes made to the test configuration. The complete LPC test article model, with the as-fabricated structural design and all component models integrated, is shown in Figure 18.
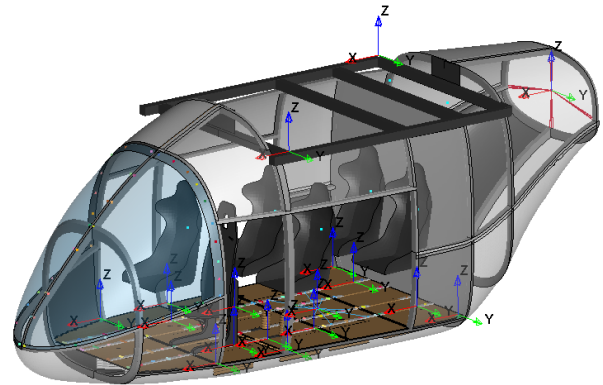

Figure 18. Complete LPC test article setup with lifting hardware.

Accelerometers were added to the model to replicate the instrumentation within the test article. Accelerometer models were attached to the floor at each A-Pillar and rear cabin frame location, at the base of each seat, and at the aft DAS location. Accelerometers were also included on the belly skin, lifting hardware, tail, and under each seat pan. The complete test article model contained 926k shell elements, 25k solid, and 117 CNRB elements with a total of 955k nodes.

RESULTS: LPC TEST MODEL CORRELATION

The LPC test was conducted at the NASA LaRC Landing and Impact Research Facility. The test article was swung onto a concrete surface with an impact velocity of 38.1 ft/s horizontal and 31.4 ft/s vertical. Using high-speed photogrammetry, the test article was measured to have an approximately 1° pitch and 2° yaw at the time of impact. To simulate the test environment a representative concrete surface model was generated. The concrete was modeled as a 410-in. x 200-in. x 24-in. block of solid elements with a mesh length varying from three to five in., increasing through the depth of the block, and a linear elastic material model. Initial velocity and vehicle orientation conditions were prescribed to the model matching those recorded at impact.

Within this manuscript both pre-test and post-test model predictions are compared with the LPC test results. The pre-test model was evaluated to identify both the capabilities and limitations associated with prediction of composite airframe crashworthiness using FE analysis. The post-test

model was developed by incorporating data obtained from the full-scale test and was evaluated to identify the effectiveness of using full-scale test data to improve crashworthiness prediction capability. The pre-test model used a notional static and dynamic contact friction between the test article and impact surface of 0.6. The high friction value was selected to represent friction effects due to tearing and grabbing of the vehicle shell against the impact surface which may not be captured within the fidelity of the test article model, as has been observed in previous full-scale fuselage impact test correlation analyses [10**Error! Reference source not found.**]. This notional friction coefficient was re-examined in the post-test model.

All simulations were performed using LS-DYNA SMP version R13.10 on a Linux computer cluster. The pre-test model was simulated to a termination time of 0.3 seconds using eight processors and had an approximate run time of 82 hours. Both test and simulation vehicle acceleration data were filtered at CFC 60 per SAE J211 recommendations for total vehicle comparison [11].

A comparison test image sequence between the LPC test article and pre-test model predictions is shown in Figure 19. The test image sequence shows the structural response of the test article to the impact load during the first 0.30 s of the impact event. From the point of impact until approximately 0.10 s, the pre-test model resembled the shape observed in the test article. Similar levels of deformation were observed in both the mid and aft door frames. In addition, the skin buckling observed in the top-front and bottom-aft skin sections was predicted by the model. After 0.10 s brittle failure of the composite airframe structure began to have an observable effect on structural deformation at multiple locations throughout the test article. This is observed in the 0.20 s and 0.30 s time sequence images, during which the brittle failure of the composite structure can be seen to cause the overhead mass to continue to compress the cabin structure. The extent of the composite material failure was not captured in the pre-test model. The model predicted the composite material to rebound elastically after the peak deformation shown in the 0.10 s image sequence. This difference between test and simulation indicated that the failure parameters within the C/C structural material model needed further calibration to better predict the brittle material failure observed during test.
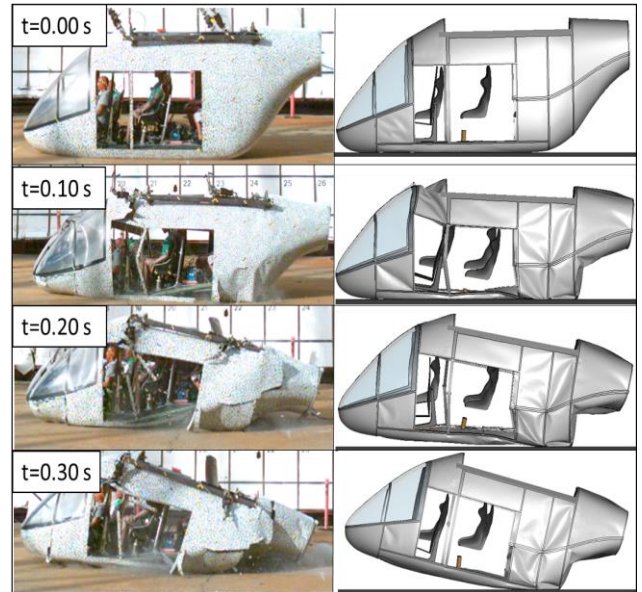

Figure 19. Test image sequence comparison to pre-test model simulation.

The first attempt at post-test model calibration examined the effect of the SLIMS and ERODS parameters of the *MAT_58 material model defining the C/C material. Post-test, these were tuned to improve the prediction of brittle failure observed in the LPC test. The coupon testing performed on the structural composite material used in the LPC test article provided data to define the linear elastic and strength parameters within the *MAT_58 material model but did not provide data to calibrate material failure response under dynamic loading. The SLIMS and ERODS parameters used to define damage and failure response of the C/C material were taken from a model of a composite material with similar carbon weave but different resin system which was previously calibrated through both coupon and component level dynamic impact level testing [5,6]. The SLIMS parameters define the magnitude by which material strength is reduced after the peak stress limit is reached in each fiber direction. A SLIMS value of 0.8 was defined in both compression and tension in the pre-test model. ERODS defines the strain value at which elements of the given material will erode during simulation. ERODS was set to 0.5 in the pre-test model. Tuning these parameters to capture the material failure observed in test resulted in a calibrated SLIMS value of 0.5 and a ERODS value of 0.15. Reduction of these parameter values during calibration was shown to significantly improve prediction of the brittle composite failure observed within the test, though there is room for further refinement. Additional component level testing of the as-fabricated material system is planned to further refine the calibrated material model parameters.

Two additional changes were made between the pre- and post-test model. The friction value, defined between the LPC test article and concrete impact surface was calibrated to 0.4. This was done to improve correlation to the slide out response observed in the test. Lastly, the point-masses used to represent the ATD weights within the seats were replaced with full ATD models in five of the six seat locations. During post-test analysis, replacing the point masses with ATD models was found to alter the predicted structural responses of the vehicle. Rigidly fixing the ATD mass to the seat was found to alter the timing of load transferred into the floor structure compared to the physical ATDs. This impact timing is dependent on both separation of the ATD from the seat during free-fall and the compression of the ATD pelvis foam material. The predicted response of the LPC structure within the tested conditions was sensitive to the slight changes in load distribution of this timing effect. Thus, the assumption that the ATD weights could be simplified using point masses for the structural evaluation of the test article was re-examined in the post-test model. To represent the physical ATDs, the LSTC Hybrid III -5th version 160920_V2, -50th version 151214_BETA, and -95th version 151214.V3.03_BETA were integrated into LPC model. Although Hybrid III FAA 50th and Hybrid II 50th ATD configurations were used in the test, the Hybrid III 50th model, which is in the automotive configuration, was used in simulation due to model availability. Although this model differs in spinal configuration from the FAA and Hybrid II versions, it accurately represented the weight distribution of these ATD configurations. In addition, when artificially positioned in an upright spinal posture using the ATD positioning tree within LS-DYNA, the LSTC Hybrid III automotive 50th model has been shown to provide a realistic prediction of lumbar load within vertical loading environments [12]. The Hybrid III 10 YO was not included within the model because a representative model of this ATD configuration was not available to the researchers at the time of this assessment. Each representative ATD model was positioned into the respective seat model to qualitatively match 3D scans taken of the LPC test article prior to the test. Representative mixed beam and shell element belt models were also generated to match the test setup.

To represent the positioned ATDs within the seat prior to impact a 0.10 s pre-load stage was added to the post-test model simulation. During this pre-load stage the vehicle model was rigidly fixed at the lifting hardware attachment while the ATD models were allowed to load into the seats under gravity. At the same time the belts were tensioned to 10 lb. to achieve a tight fit between belt and ATD. The impact velocity was then applied resulting in the pre-load phase through impact event being replicated through a continuous simulation. The post-test model was simulated to a termination time of 0.4 s, including the pre-load phase,

using eight processors and had an approximate run time of 173 hours.

Comparisons image between the test and the post-test LPC model at simulation completion are shown in Figure 20. The calibration of the composite material damage and failure parameters within the post-test model was shown to improve prediction of the cabin collapse observed in the LPC test. Reducing the strain threshold at which the material model eroded elements resulted in a more realistic prediction of the brittle material failure test at peak structural deformation observed in. The reduced strain threshold led to improved prediction of the structural frames at the center and aft door frame location snapping as they did in the test article rather than rebounding elastically as they did in the pre-test model. These results stress the importance of calibrating the failure characteristics of composite material models under relevant dynamic loading conditions to realistically predict structural response in crash simulation analysis.

Figure 20. Post-test model prediction of cabin damage.

A comparison of acceleration response measured on the test article lifting hardware to that predicted by the pre- and post-test model configurations is shown in Figure 21. Acceleration comparisons are made over the first 0.15 seconds of impact. Minimal acceleration response was recorded in the structure after this time. Acceleration predictions are shown only in the vertical direction because horizontal acceleration loading was minimal within the vehicle structure. Both the pre- and post- test model show very similar prediction of the acceleration measured in the lifting hardware. Acceleration was closely predicted over the initial impact load. An acceleration spike was measured at 0.10 s which was not captured by either model. This spike was likely caused by internal contact with the lifting hardware and an ATD within the test article which is highly sensitive to the ATD motion being perfectly predicted with respect to the cabin structure. Close and similar prediction of the lifting hardware acceleration by both models verifies good correlation of the both the pre- and post-test LPC material model prior to failure.
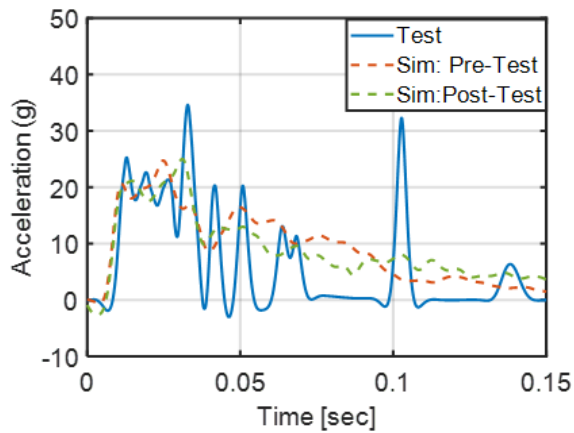

Figure 21. Lifting hardware vertical acceleration.

Prediction of A-pillar vertical acceleration responses in the pre- and post-test models are shown in Figure 22. Both models predict the acceleration response measured in the test article, while the post-test model showed improved prediction of the initial peak acceleration. A large acceleration spike was observed at approximately 0.03 seconds in the starboard A-pillar accelerometer. This acceleration spike is indicative the accelerometer contacting either the vehicle structure or ATD component and not directly relevant to the structural loading prediction being evaluated.
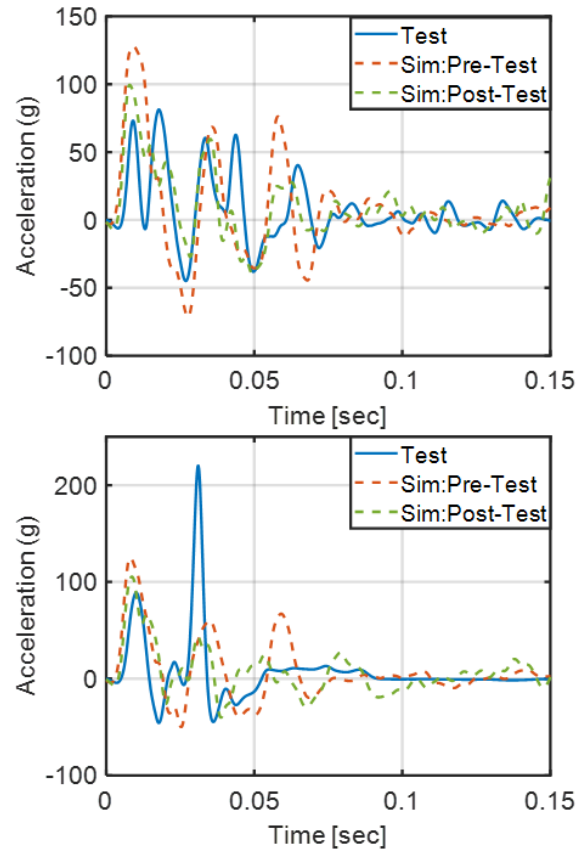

Figure 22. A-pillar vertical acceleration: Portside (top) and starboard (bottom).

Prediction of vertical acceleration measured at the DAS location on the floor is shown in Figure 23. Acceleration response at the location is precisely predicted by the post-test model while the pre-test model slightly overpredicts the initial acceleration spike and subsequent oscillations. Precise prediction in the post-test model can be attributed to the greater reduction in composite material stiffness with damage applied in the post-test calibrated model. This reduced stiffness with damage progression slightly reduced the initial peak acceleration predictions measured within the cabin to bring them more in-line with that measured in the test.
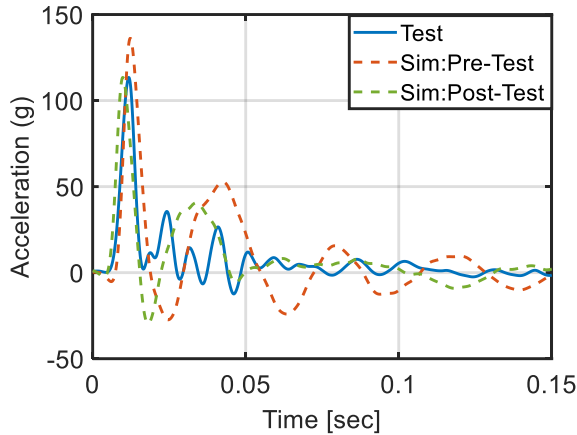
Figure 23. Floor DAS location vertical acceleration.

Prediction of under-seat floor vertical accelerations measured along the length of the test article are shown in Figure 24. A more significant difference between pre- and post-test model acceleration predictions were observed in the seat area locations than the other locations within the test article. The post-test model exhibited improved prediction of acceleration shape and peak value compared to the pre-test model, particularly in the mid and aft seat locations. This difference is driven by the de-coupling of the occupant mass from the vehicle structure in the post-test model. This de-coupling changed the timing in which the occupant mass compresses into the floor and energy absorbing subfloor structure. In the post-test model the mid and aft starboard occupants are represented by ATD models, matching the ATDs used in test. The H3 10 YO ATD in the forward starboard seat was represented by a rigid point mass in both models, due to lack of model availability for this ATD configuration. The H3 10 YO has the lowest mass of ATDs tested and the mass simplification effect was minimal. The aft starboard seat contains the heaviest mass, H3 95th ATD, and thus the greatest difference between pre- and post-test model correlation is observed in this location.
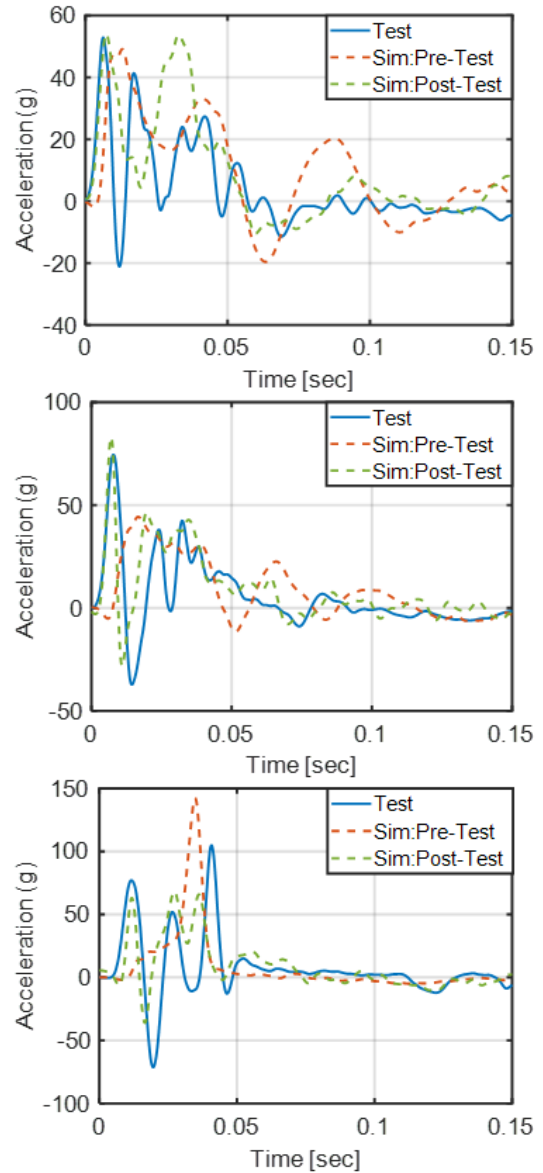

Figure 24. Starboard floor vertical acceleration: Front (top), mid (middle), and aft (bottom).

Prediction of seat vertical accelerations measured along the length of the test article are shown in Figure 25. Similar to the under-seat floor locations, inclusion of the ATD models within the full impact simulation was shown to improve acceleration predictions. Correlation in the front starboard seat, in which the occupant was represented by a point mass in both models, decreased in the post-test model. Reduced peak acceleration was predicted by the post-test model which was likely driven by the increased stiffness reduction due to damage effect seen in other structural locations. Replacing point masses with full ATD models was shown to increase peak initial acceleration prediction in the other seat locations, and thus it can be assumed that the use of a representative 10 YO ATD model would improve seat

acceleration correlation in this location. Acceleration shape is well predicted by the post-test model in the mid and aft seat locations, though the mid location slightly overpredicts the initial peak.
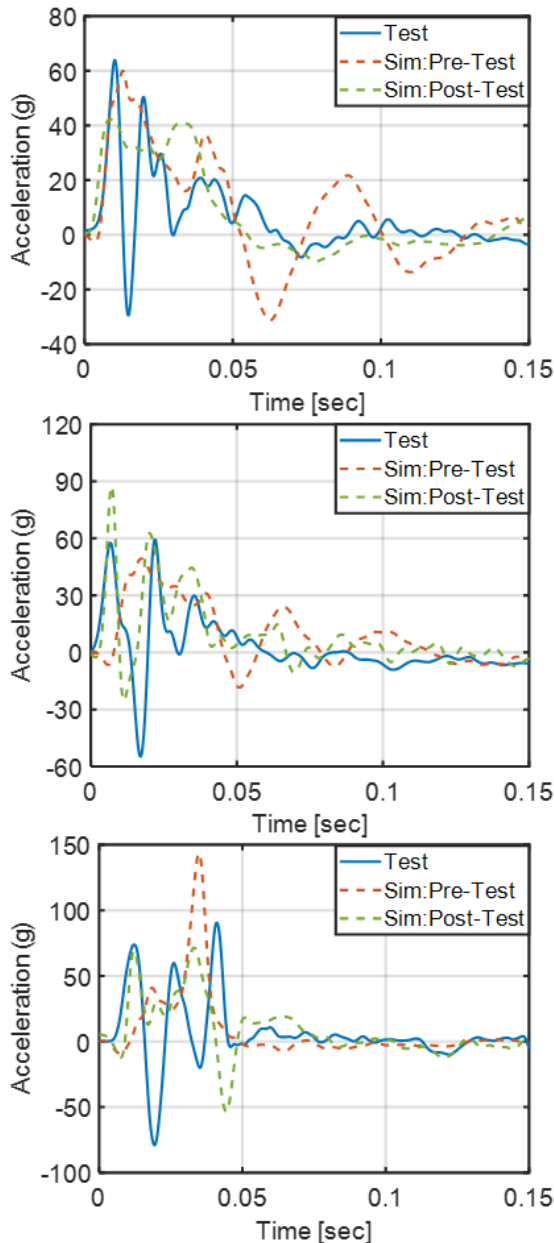

Figure 25. Starboard seat pan vertical acceleration: Front (top), mid (middle), aft and (bottom).

The prediction of lumbar load response was evaluated to determine the capability of the developed model to accurately predict occupant injury risk within the dynamic loading environment. Peak compressive lumbar load in the H3 50th ATD is the current standard metric used to assess spinal injury risk due to vertical loading within FAA certification requirements for rotorcraft [13]. Current

certification requirements specify a cutoff value of 1,500 lb. of compression force measured in the lumbar spine load cell. In the LPC test, two H3 50th ATDs were seated in the mid-section of the test article, one in a rigid framed seat and one in the NASA EA seat. The H3 50th in the rigid seat recorded a peak lumbar load well above the certification limit, while the EA seat was found to reduce the lumbar load to below the limit. The ATD models integrated into the post-test vehicle model were found to accurately predict the lumbar load values measured in each seat configuration, this is shown in Figure 26. The lumbar load predicted in the rigid seat exhibited a drop at approximately 0.02 s, which was not seen in the test, though it quickly rebounds and tracks the shape and magnitude of the measured response. The lumbar load in the EA seat closely tracks the measured test response during the first 0.05 s of impact, though it does not unload as quickly as what was measured in test. Overall, the model accurately captures the effect of the developed EA mechanisms on occupant injury risk which gives confidence in using these models to further optimize the EA designs under expanded loading environments.
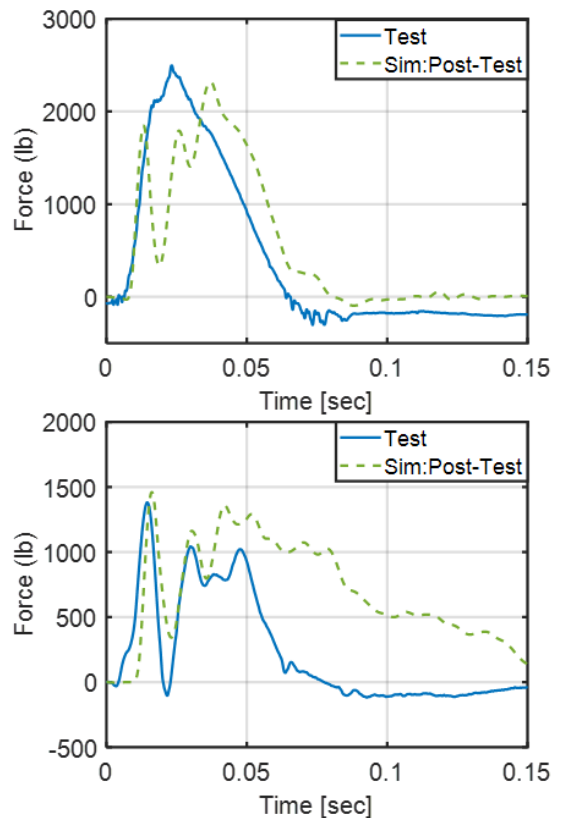

Figure 26. H3 50th lumbar load time history in rigid (top) and NASA EA (bottom) seats.

CONCLUSIONS

The dynamic impact test performed on the NASA LPC vehicle configuration was carried out to improve eVTOL occupant safety by furthering understanding of composite airframe structural response within the crash impact environment, verifying the capability of novel EA components developed for integration into eVTOL vehicle design, and quantifying the predictive capability of analytical tools used to study vehicle crashworthiness. This manuscript describes the development of a FE model of the test article and examines the correlation of model predictions to test results. This work was conducted to improve understanding of analytical predictive capability as well as provide lessons learned for future endeavors into eVTOL crashworthiness simulation.

The FE model of the LPC test article was developed to match the as-fabricated design as close as possible given the fabrication specifications and material test data available. Component assembly and bond lines defined within the fabrication process were replicated in the model. A model of the structural composite material was generated using static coupon testing. Models of the EA components integrated within the test article were generated and validated prior to the test through both coupon material testing and component level dynamic impact tests. Comparison of pre-test predictions and test results identified both capabilities and limitations of the FE model to quantify crashworthiness of an eVTOL relevant vehicle design.

Simulation of the test conditions using the pre-test vehicle model showed the model was capable of predicting acceleration loads transferred through the vehicle structure but was not effective at predicting the survivable volume of the structure post-impact. The primary acceleration load transferred into the vehicle structure occurred over the first 0.05 s post-impact. The primary acceleration occurred before the majority of brittle failure of the composite structure occurred, and thus the predictive accuracy observed during this time can be associated with accurate pre-failure parameters defined within the structural composite material model. These parameters were defined using the coupon material testing performed prior to the full-scale test. The survivable volume of the vehicle was not predicted by the pre-test model because it did not predict the brittle fracture of the structural material which occurred during the test. Compared to the elastic-plastic-fracture response of metallics used in traditional aircraft structures, carbon composite materials can have a sharp transition between elastic response and brittle failure. This sharp transition was observed in the LPC test article and lead to structural failure and partial loss of survivable volume. Tuning the failure parameters within the composite material model led to improved prediction of the brittle failure

observed in test. These results indicate the importance of performing tests to thoroughly characterize the sensitivity of composite material failure parameters to the loading environments over which it will be used. This characterization is necessary to provide confidence in any assessment of vehicle survivable volume through FE analysis.

The test article structure had been sized to meet CFR 27.561 load requirements through FE analysis. Although the limitations in material model failure parameter calibration was a significant contributor to the failure of the test article not being identified in this sizing analysis, there are additional discrepancies between the sizing analysis and the final test article that may have also contributed. First, the preliminary sizing analysis did not account for fabrication effects on the structural response of the test article. Aspects such as bond-line locations and small geometric changes occurring during fabrication and assembly can contribute to differences in structural response under load. In addition, the wing mass integration was redesigned during test article buildup to improve test safety. Although these changes were integrated into the pre-test model and analysis of the to-be-tested conditions indicated cabin volume retainment, a second sizing analysis was not performed with the updated design prior to test. The resulting cabin structural failure indicates the importance of iterative process in vehicle design in which structural sizing should be re-assessed as the design is matured and material response characterization is improved.

The EA component models, of which the C/K material system had been thoroughly characterized through both static coupon and dynamic component level tests to failure, were found to accurately predict component response within the tested environment. Seat and floor level accelerations, which were driven by a combination of vehicle structure and component responses, were both well predicted through simulation. During evaluation of the floor and seat response predictions it was found that the initial assumption that the ATDs used in test could be represented by rigid masses without altering prediction of vehicle structural response, was incorrect for this vehicle. Often in vehicle level impact simulations occupants are represented as point masses, and breakout simulations of each seat and occupant are performed separately to optimize computation time [14]. The ATDs used in the LPC test accounted for approximately 1/3 of the total weight of the test article. The high relative mass of the occupants and multiple EA components between airframe and seat, which were found to be sensitive to timing of seat/occupant mass interaction, drove the importance of ATD model inclusion within the vehicle simulation.

Based on the correlation of the pre-test LPC model to the full-scale test results, two major modelling lessons learned

were identified. These lessons learned can be summarized as:

- Calibration of composite material and failure parameters, specific to the composite construction and dynamic loading environment the vehicle structural model is intended to evaluate, are necessary to fully predict aircraft structural response throughout the impact event. Dynamic material testing of as-fabricated component specimens is recommended to improve predictive accuracy of composite failure prior to full-scale validation testing.

- ATD weight cannot be simplified as point masses in all vehicle simulation analyses. Verification simulations should be performed in which both representative occupant and point masses are simulated. If differences in predicted acceleration at seat attachment is observed than simulation with full ATD models is recommended.

The post-test model of the LPC test article which included calibration of the composite structure material model failure parameters and full ATD models, was shown to effectively predict airframe structural response as well as occupant injury risk measured during test. Occupant injury risk, quantified through H3 50th compressive lumbar load, was closely predicted using the post-test model for both rigid and EA seat configurations. These results lend confidence in the capability of FE modeling to predict occupant injury risk within eVTOL relevant airframe designs when the models are properly grounded in test data.

To validate the modeling lessons learned and explore the effect of design changes on structural response, NASA is planning to test a second LPC test article. The LPC model developed in the current study will be used to identify design improvements as well as predict the sensitivity of the vehicle to new loading conditions. Predictions will be used to guide the second test conditions. Test results will be used to quantify the capability of the FE model to predict response in conditions not directly calibrated too. Results of this work are intended to provide vehicle manufacturers and standards organization data on the capability and limitations of FE model analysis used to make vehicle crashworthiness predictions for eVTOL vehicle design.

AUTHOR CONTACT

Jacob Putnam - Jacob.b.putnam@nasa.gov

Justin Littell - justin.d.littell@nasa.gov

REFERENCES

1. Silva, C., Johnson, W., Antcliff, K.R., Patterson, M.D., "VTOL Urban Air Mobility Concept Vehicles for Technology Development," Proceedings from the 2018 Aviation Technology, Integration, and Operations Conference, Atlanta, GA, June-25-29, 2018.

2. Littell, J.D., Putnam, J.B., Cooper, M., "Simulation of Lift plus Cruise Vehicle Models to Define a Full-Scale Crash Test Campaign," Proceedings from the Vertical Flight Society 77th Annual Forum and Technology Display, May 12, 2022

3. Federal Aviation Administration, "Emergency Landing Dynamic Conditions," 14 CFR § 27.561, Amended November 13, 1989.

4. American Society for Testing and Materials, "Standard Test Method for Tensile Properties of Polymer Matrix Composite Materials," ASTM-D3039M, 2008.

5. Jackson, K.E., Fasanella, E.L., and Littell, J.D., "Development of a Continuum Damage Mechanics Material Model of a Graphite-Kevlar ® Hybrid Fabric for Simulation the Impact Response of Energy Absorbing Subfloor Concepts," Proceedings from the 73rd Annual American Helicopter Society Annual Forum and Technology Display, Fort Worth, TX, May 9-11, 2017.

6. Littell, J. and Putnam, J., "The Evaluation of Composite Energy Absorbers for use in UAM VTOL Vehicle Impact Attenuation," Proceedings from the 75th American Helicopter Society Annual Forum and Technology Display, Philadelphia, PA. May 13-16, 2019.

7. Putnam, J.B. and Littell, J.D., "Evaluation of Impact Energy Attenuators and Composite Material Designs of a UAM VTOL Concept Vehicle," Proceedings from the 75th Vertical Flight Society Annual Forum and Technology Display. Philadelphia, PA, May 13-16, 2019.

8. Putnam, J.B. and Littell, J.D., "Crashworthiness of a Lift plus Cruise eVTOL Vehicle Design within Dynamic Loading Environments," Proceedings from the Vertical Flight Society 76th Annual Forum and Technology Display, October 5-8, 2020.

9. Putnam, J.B., Littell, J.D., Reaves, M., "Development and Analysis of Energy Absorbing Subfloor Concepts to Improve eVTOL Crashworthiness," Proceedings from the Vertical Flight Society 78th Annual Forum and Technology Display, Fort Worth, TX. May 2022.

10. Jackson, K.E., Putnam, J.B., "Simulation of a Full-Scale Crash Test of a Fokker F28 Fellowship Aircraft," NASA/TM–2020-220435, January 2020.

11. Society of Automotive Engineers (SAE), "Surface Vehicle Recommended Practice: Instrumentation for Impact Test-Part 1-Electronic Instrumentation," SAE J211-1, 2017

12. Putnam, J.B., Somers, J., Wells, J., Newby, N., Siders, B., Currie Gregg, N., Lawrence, C., "Evaluation of Mid-Size Male Hybrid III Models for use in Spaceflight Occupant Protection Analysis," SAFE Journal, 38.1 (2018): 10-33.

13. Federal Aviation Administration, "Emergency Landing Dynamic Conditions." 14 CFR § 27.561, Amended November 13, 1989.

14. Putnam, J.B., "Occupant Response Analysis of a Full-Scale Crash Test of a Fokker F28 Fellowship Aircraft," NASA/TM–2020-220571, March 2020.